

# Experimental Verification of Sub-wavelength Focusing Via a Holographic Metallic Screen

Alex M. H. Wong\* and George V. Eleftheriades  
Edward S. Rogers Sr. Department of Electrical & Computer Engineering,  
University of Toronto, 10 King's College Road, Toronto, Ontario, M5S3G4, Canada.

## Introduction

Since the introduction of the notion of a perfect lens by Pendry [1], there has been considerable interest and work on near-field sub-wavelength focusing structures [2]-[3]. In particular, near-field sub-wavelength focusing has been demonstrated by artificially synthesized metamaterial lenses, which more or less operate under the perfect lens concept. While these structures indeed hold promise to various applications such as microwave imaging, near-field sensing, lithography, microscopy, etc., various loss mechanisms limit their practical focusing capability from reaching far beyond the diffraction limit [4]. In this paper we present experimental verification of sub-wavelength focusing based on an entirely new concept: the holographic metallic screen [5]-[7]. This screen involves an array of closely spaced slot antennas [6], and exploits resonance to boost the field magnitude of the sub-wavelength focus [7].

## Theory and Formulation

For completeness, we offer a brief conceptual overview of the screen design procedure, which has already been thoroughly described in [7]. Fig. 1 shows the geometry we will consider in our formulation. We begin by seeking a field distribution at the screen,  $E(x, z = -s - d)$ , which would generate a highly focused 2D field distribution

$$E(x, z = -s) = \exp(-ikr) / r \quad (1)$$

where  $r = \sqrt{x^2 + s^2}$  at the image plane  $z = -s$ . Back-propagating the electric field via a spectral decomposition method yields the corresponding spectrum at the plane of the screen,

$$S(k_x, z = -s - d) = K_0(|k_x|s) \exp(|k_x|(d + s)) \quad (2)$$

where  $K_0$  is the zeroth-order modified Bessel function of the 2nd kind. The above spectrum is dominated by high spatial frequency components. Furthermore, it is physically unrealizable since  $\exp(|k_x|(d + s))$  becomes unbounded as  $|k_x| \rightarrow \infty$ . Hence we consider a band-limited spectrum  $S'(k_x)$ , which equals  $S(k_x, z = -s - d)$  for a limited spectral band  $|k_x| \leq |k_m|$ , but vanishes outside this band. We then apply a high spatial frequency asymptotic approximation to  $S'(k_x)$  to analytically express the field distribution at the screen as,

$$E_{apr}(x) = \frac{\exp(k_m d) \cos(k_m x)}{d^2 + x^2}. \quad (3)$$

By synthesizing this field distribution at the plane of the screen, we can recreate a close approximation of (1) at the image plane, and thereby produce a sub-wavelength focus.

We can reconstruct (3) borrowing concepts from holography. In holography, one makes a complete record of an object wavefront by interfering it with a reference wavefront. We choose a normally incident plane wave as our reference wave, and express the holographic interference at the screen as,

$$T(x) \propto 1 + 2 \operatorname{Re}\{E_{obj}(x, z = -s - d)\} + |E_{obj}(x, z = -s - d)|^2. \quad (4)$$

As explained in [6], to eliminate the constant transmission background, we suppress all terms but the second in (4) to obtain (5). We are fortunate that our object wavefront (3) is already real, so (5) readily simplifies to (6). Nevertheless, (5) would apply for a general  $E_{appr}(x)$ , analytically or numerically solved for an arbitrary image field distribution.

$$T(x) \propto \operatorname{Re}\{E_{obj}(x, z = -s - d)\} \quad (5) \quad T(x) \propto E_{appr}(x). \quad (6)$$

We propose using an array of slot antennas over an infinite ground plane to convert a normally incident plane wave into the function  $T(x)$  as specified in (6). Since a slot antenna of a length below half wavelength is inductive, and one of length above half wavelength is capacitive, the respective radiated fields from these antennas will be  $\pi$ -shifted in phase, generating a sign change in  $T(x)$ . Furthermore, the field radiated from a slot antenna strengthens (or weakens) as its length gets closer to (or farther from) the half wavelength resonance. Thus by controlling the slot dimensions to be above or below, and close to or far from resonance (nominally at half wavelength), one can reconstruct an arbitrary  $T(x)$  upon normal plane wave incidence.

## Design and Fabrication

Following the formulation outlined above, we have designed a metallic transmission screen which tightly focuses a 10GHz incident plane wave at a distance of 4.5mm (0.15-wavelength) away from the screen. We chose  $k_m = 5k_0$ , which should lead to a fivefold focal width improvement over a far-field diffraction-limited distribution. For simplicity, and inspired by calculations from [7], we designed the screen using only three slots (a 1.2mm x 13.2mm central slot, and two 0.6mm x 17.0mm side slots), as opposed to an infinite array of slots. These slots were spaced a 3mm (0.1-wavelength) apart; the central slot, which synthesized the positive peak of  $T(x)$  at  $x = 0$ , was slightly shorter than half-wavelength, while the side slots, which synthesized the negative peaks of  $T(x)$  at  $x = \pm 3$  mm, were slightly longer than half-wavelength, but farther from the half-wavelength resonance so as to give a weaker transmission magnitude in comparison to the central slot. Fig. 1 shows a diagram of the designed screen. Simulation using Ansoft's HFSS showed that the x-directed electric field (the dominant component of the electric field) forms a focus of only 4.9mm, or 0.16-wavelength (electric field FWHM) at the image plane. Thus one can achieve superb focusing capability even with very few slots.

The screen was fabricated by laser-cutting the designed slots from a stainless steel plate of a thickness of 6mil (0.152mm). The stainless steel plate was then stretched onto a frame to ensure its flatness.

## Experimental Results

### A. Apparatus

Fig. 2 shows a schematic of our experimental apparatus. Port 1 of an Agilent E8364B Performance Network Analyzer (PNA) drove an X-band horn, transmitting a spherical wave with the E-plane aligned in the x-direction; this wave was collimated by a Rexolite dielectric lens to form a Gaussian beam which closely approximated plane wave incidence at the screen. On the output side of the screen, the x-directed E-field was detected by a dipole probe, which was connected to port 2 of the PNA. The dipole probe was made from a EZ47 semi-rigid co-axial cable by Huber + Suhner; details of its orientation within the apparatus are shown in Fig. 2. We performed three automated  $S_{21}$  scans with this apparatus: 1) a scan over the image plane, with all 3 slots unobstructed; 2)

a scan over the image plane with the two side slots covered with copper tape, leaving only the central slot; and 3) a scan without the screen for calibration purposes.

### B. Sub-wavelength Focusing

Fig. 3 shows the experimentally measured  $E_x$  field distribution at the  $y = 0$  line over the image plane (solid line), compared alongside the same experimental measurement with the side slots covered (dash line), and a corresponding simulation using Ansoft's HFSS, where the metal ground plane is simulated as a perfect electric conductor (dotted line). The measured field distribution is asymmetric due to an unwanted direct coupling of fields into the co-axial cable. This spurious coupling was most severe when the co-axial cable was closest to the central slot, which correspondingly smoothed the +x direction of the plot, as can be deduced from the probing geometry shown in Fig. 2. Despite this asymmetric smoothing caused by probe imperfection, the FWHM of the electric field measures 5.2mm, or 0.17-wavelength – which agrees well with the simulation value of 0.16-wavelength, and shows a clear improvement from the FWHM of 9.8mm, or 0.33-wavelength obtained with the side slots covered. The excellent agreement between the measured focal width and the simulated focal width (where again, a PEC is used instead of a metallic ground plane) verifies that the focusing quality is minimally affected by conductive loss in the stainless steel ground plane. In this respect, our proposed screen is advantageous over most existing resonance-dependent subwavelength focusing structures, including metamaterial lenses, which suffer from a resolution limitation caused by losses accompanied by implicated resonances [2], [4].

### C. Resonant Enhancement of the Transmitted Electric Field

Another merit of this subwavelength focusing screen which deserves special remark is its ability to enhance the electric field strength at the image plane. Since subwavelength focusing structures generate evanescent waves which rapidly decay towards the image plane, the field strength is often much weaker at the image plane than at the output surface of the structure. In this regard, our proposed metallic screen is no different. However, for our metallic screen, the resonant field coupling from the incident plane wave to the slot antennas boosts the field strength at the image plane, making the focal point field strength comparable, or even stronger, than that of the incident wave. Fig. 4 compares the simulated and measured electric field distributions at the image plane, with both of them normalized to the incident electric field  $E_0$ . Besides a slight attenuation, the experimental measurement closely matches the result from the corresponding full-wave simulation with a PEC screen. The measured peak field strength is 1.05 times the field strength of the incident plane wave, verifying our screen's ability to enhance the field transmitted electric field.

## Conclusion

In this paper we have experimentally demonstrated the viability of a subwavelength focusing screen, formed by placing slot antennas over a ground plane. In a proof-of-principle experiment using only 3 slots, we have focused the x-directed E-field to a FWHM of 5.2mm (0.17-wavelength) at an image plane 4.5mm (0.15-wavelength) from the screen at  $f = 10$  GHz. Our measured results indicate that the screen's focusing quality and the electric field intensity at the focal spot are only minimally affected by conductor losses. We have also verified that resonant coupling enhances the peak field intensity at the focal spot to a level comparable to the incident field. The loss independence and high transmitted peak intensity make our subwavelength focusing screen an attractive option for practical subwavelength focusing in the near-field.

## References

- [1] J.B. Pendry, "Negative Refraction makes a perfect lens," *Phys. Rev. Lett.*, April 2000, 85, (18) pp. 3396-3969.
- [2] A. Grbic and G. V. Eleftheriades, "Overcoming the diffraction limit with a planar left-handed transmission-line lens," *Phys. Rev. Lett.*, March 2004, vol. 92, no. 11, pp. 117403.
- [3] M.J. Freire and R. Marqués, "Planar magnetoinductive lens for three-dimensional subwavelength imaging," *Appl. Phys. Lett.*, April 2005, vol. 86, pp. 182505.
- [4] A. Grbic and G.V. Eleftheriades, "Practical limitations of subwavelength resolution using negative-refractive-index transmission-line lenses," *IEEE Trans. Antennas Propag.*, Oct. 2005, vol. 53, no. 10, pp. 3201-3209.
- [5] G.V. Eleftheriades, "Negative-Refractive-Index Transmission-Line (NRI-TL) Metamaterials," *Intl. Symposium on Electromagnetic Theory URSI-Commission B*, Ottawa, July 26-28, 2007.
- [6] A.M.H. Wong, C.D. Sarris and G.V. Eleftheriades, "Metallic transmission screen for sub-wavelength focusing," *IEE Electronics Letters*, vol. 43, no. 25, pp.1402-1404, Dec. 2007.
- [7] G.V. Eleftheriades and A.M.H. Wong, "Holography-Inspired Screens For Sub-wavelength Focusing in the Near Field," Accepted in *IEEE Microwave Wireless Comp. Lett.*

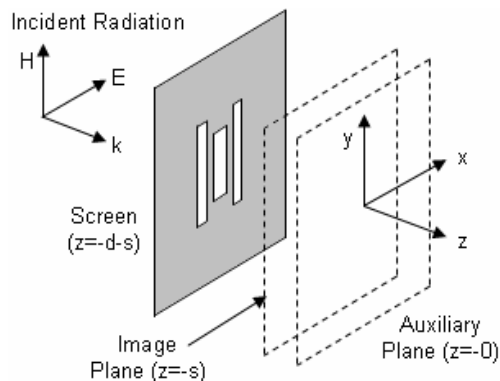


Fig. 1: A schematic diagram of the metallic sub-wavelength focusing screen.

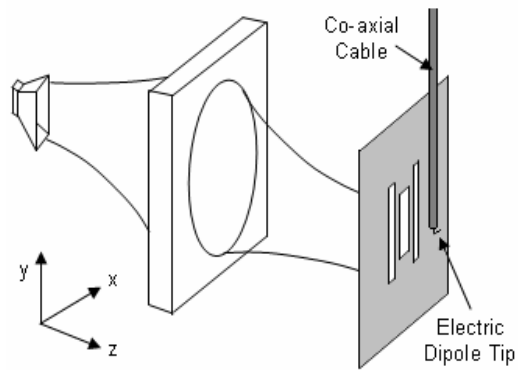


Fig. 2: A schematic of the experimental apparatus.

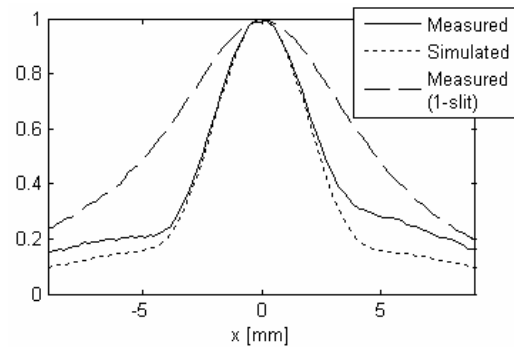


Fig. 3: A plot of  $|E_x|$  (normalized) along the  $y=0$  line on the image plane.

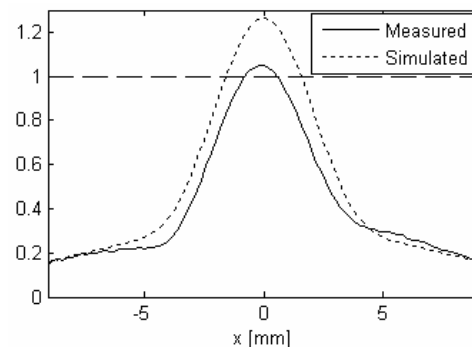


Fig. 4: A plot of  $|E_x| / |E_0|$  along the  $y=0$  line on the image plane.